Heterogeneous & Homogeneous & Bio- & Nano-

CHEMCATCHEM

CATALYSIS

Accepted Article

Title: Effect of oxide support on catalytic performance of FeNi-based catalysts for CO2-assisted oxidative dehydrogenation of ethane

Authors: Binhang Yan, Siyu Yao, and Jingguang G. Chen

To be cited as: *ChemCatChem* 10.1002/cctc.201901585

Link to VoR: http://dx.doi.org/10.1002/cctc.201901585

A Journal of

ChemPubSoc Europe

WILEY-VCH

www.chemcatchem.org

10.1002/cctc.201901585

Effect of oxide support on catalytic performance of FeNi-based catalysts for CO_2-assisted oxidative dehydrogenation of ethane

Binhang Yan, [a, b] Siyu Yao, [b] and Jingguang G. Chen *[b, c]

[a] Prof. Dr. Binhang Yan

Department of Chemical Engineering

Tsinghua University

30 Shuangqing Rd. Haidian District Beijing, 100084 (China)

[b] Prof. Dr. Binhang Yan, Prof. Dr. Siyu Yao, Prof. Dr. Jingguang G. Chen

Chemistry Division

Brookhaven National Laboratory

55 Lewis Rd. Upton NY, 11973 (USA)

[c] Prof. Dr. Jingguang G. Chen

Department of Chemical Engineering

Columbia University

500 W. 120th St. New York NY, 10027 (USA)

Telephone: (212) 854-6166, Fax: (212) 854-3054

Email: jgchen@columbia.edu

ABSTRACT

CO_2-assisted oxidative dehydrogenation of ethane over Fe_3Ni_1 catalysts supported on SiO_2, ZrO_2, and CeO_2, as well as CeO_2-supported $Fe_{3x}Ni_x$ with different metal loadings (x = 0.25, 0.5, 1, 2, 4), were investigated to illustrate the effects of the oxide support and the metal loading amount in tuning the catalytic activity and selectivity. The oxidation state and the dispersion of the Ni and Fe species on the supported catalysts were determined by using *in-situ* X-ray diffraction (XRD) and X-ray absorption fine structure (XAFS) measurements. Among these FeNi-based catalysts, Fe_3Ni_1/CeO_2 exhibited the best catalytic activity and maximum ethylene yield for the oxidative dehydrogenation of ethane. Excessive loading amount of active metals changed the reaction selectivity from oxidative dehydrogenation to dry reforming. The high activity and selectivity for CO_2-assisted oxidative dehydrogenation of ethane over Fe_3Ni_1/CeO_2 are likely due to the formation of Ni-FeO_x/CeO_x interfacial sites, while the presence of Ni-ZrO_2 interfacial sites on Fe_3Ni_1/ZrO_2 and NiFe-CeO_x interfacial sites on $Fe_{12}Ni_4/CeO_2$ likely tune the reaction selectivity toward dry reforming of ethane.

Keywords: Heterogeneous catalysis; Support effect; Oxidative dehydrogenation; Dry reforming; Selectivity

Introduction

CO_2-assisted oxidative dehydrogenation of ethane ($C_2H_6 + CO_2 \rightarrow C_2H_4 + CO + H_2O$) selectively cleaves the C-H bonds while preserving the C-C bond of ethane to produce ethylene. The reaction has attracted significant research interest [1-6] as it offers a potential way to simultaneously upgrade the underutilized ethane in the shale gas and mitigate the rising global CO_2 emission. However, the competing reaction, i.e., CO_2 reforming of ethane ($C_2H_6 + 2CO_2 \rightarrow 4CO + 3H_2$), breaks all the C-H and C-C bonds of ethane to produce synthesis gas [7-9]. The dry reforming reaction is thermodynamically more favorable under the reaction conditions. Therefore, research efforts should focus on developing new catalysts with high oxidative dehydrogenation selectivity to produce more desirable ethylene. Many attempts have been made to promote the oxidative dehydrogenation selectivity by using Ga-based oxide catalysts [10-11], Cr-based oxide catalysts [4, 6, 12-16], Co-based oxide catalysts [17-18], metal carbide catalysts [19-20], and other catalysts [21-23]. Although theses catalysts exhibit high initial dehydrogenation activity, the stability is poor, likely due to the coke formation. The improvement of the selectivity and stability of CO_2-assisted oxidative dehydrogenation of ethane requires a bifunctional catalyst that can dissociate CO_2 into CO and a reactive surface oxygen species [5, 24] and activate the adsorbed ethane on metal centers or metal-support interfaces.

The interaction between the active metal and an oxide support presents an opportunity to design new catalysts with enhanced oxidative dehydrogenation selectivity. Reducible supports (e.g., CeO_2) are commonly used as they can promote

the activation of CO_2 via direct C=O bond scission [2, 24]. The released reactive surface/lattice O atoms can readily remove the formed coke deposits and allow the overall reaction to proceed efficiently. In previous studies Fe_3Ni_1/CeO_2 was identified as a promising catalyst with high selectivity and excellent stability for CO_2-assisted oxidative dehydrogenation of ethane to produce ethylene [2, 25]. The Ni-FeO_x interfaces and Ni-CeO_x interfaces were demonstrated as the most likely active sites for the oxidative dehydrogenation pathway and the dry reforming pathway, respectively. The two types of active sites on CeO_2-supported FeNi catalysts could be further tuned to rationally manipulate the catalytic selectivity by changing the Fe/Ni ratio.

Many studies have reported that catalysts using different supports show distinctive catalytic properties [26-28]. However, the support effects of the FeNi-based catalysts on the catalytic performances of CO_2-assisted oxidative dehydrogenation of ethane, especially on the properties of the active metal species, have not been studied or fully understood. SiO_2 provides an irreducible and relatively inert substrate [28]. ZrO_2 is debatably considered to be reducible or at least partially reducible, but it is certain that the support exhibits surface defects or kinks that can strongly influence catalyst activity and selectivity [29]. CeO_2 is classified as a readily reducible oxide with ability to store and release oxygen, which not only facilitates CO_2 activation, but also provides lattice oxygen for coke suppression [30]. There is a clear need to expand the knowledge regarding the effect of oxide supports for the reaction of C_2H_6 with CO_2 to develop highly active and selective catalysts for the oxidative dehydrogenation pathway. Hence the objective of this work is to study the influences of different supports (SiO_2, ZrO_2,

and CeO_2) on the catalytic performances of Fe_3Ni_1-based catalysts, and to further understand the optimum loading amount of $Fe_{3x}Ni_x/CeO_2$ (x = 0.25, 0.5, 1, 2, 4) catalysts for CO_2-assisted oxidative dehydrogenation of ethane using a combination of flow reactors and *in-situ* XRD and XAFS characterization.

Results and Discussion

Effect of support

To explore the support effect, supported-Fe_3Ni_1 (same Fe/Ni ratios and weight loadings) catalysts with different supports (SiO_2, ZrO_2, and CeO_2) were tested at 873 K for over 13 h (10 mL/min C_2H_6 + 10 mL/min CO_2 + 20 mL/min Ar). The conversion of C_2H_6 and CO_2, the yield of C_2H_4 and CO, and the selectivity toward C_2H_4 and CO over the three supported-Fe_3Ni_1 catalysts, are shown in Figure 1 as a function of time on stream. The steady-state conversion, yield, selectivity, turnover frequency (TOF) and space-time yield (STY) are listed in Table 1. As compared in Figure 1 and Table 1, the oxide supports have remarked influence on the catalytic activity of supported-Fe_3Ni_1 catalysts.

Fe_3Ni_1/SiO_2 shows poor activity, either for the oxidative dehydrogenation reaction or for the dry reforming reaction. Severe deactivation on Fe_3Ni_1/ZrO_2 is observed: the C_2H_6 (CO_2) conversion gradually changes from 10% (27%) at the first 0.5 h to 2% (4%) after 13 h operation. The C_2H_4 selectivity is also greatly varied (from 3% to 67%) during the reaction, indicating that the selectivity evolution on Fe_3Ni_1/ZrO_2 might be due to the transformation of active sites. Compared to Fe_3Ni_1/SiO_2 and Fe_3Ni_1/ZrO_2,

10.1002/cctc.201901585

Fe_3Ni_1/CeO_2 shows an enhanced and stable C_2H_4 yield/selectivity, with an over 80% C_2H_4 selectivity. The C_2H_6 conversion, CO_2 conversion, and C_2H_4 yield over Fe_3Ni_1/CeO_2 change slightly during the reaction, suggesting that the active sites that favor oxidative dehydrogenation on the catalyst are stable. The catalytic performance over Fe_3Ni_1/SiO_2, Fe_3Ni_1/ZrO_2, and Fe_3Ni_1/CeO_2 at different temperatures varying from 873 K to 823 K after 13 h operation is compared in Figure 2. As is seen from Figure 2, the conversion of C_2H_6 and CO_2, and the yield of C_2H_4 and CO over the three supported-Fe_3Ni_1 catalysts gradually increase with the increase of temperature, while the C_2H_4 selectivity over Fe_3Ni_1/CeO_2 also changes slightly when the temperature changes. Furthermore, the C_2H_4 selectivity over Fe_3Ni_1/CeO_2 still remains comparatively steady when the gas hourly space velocity (GHSV) is changed (by varying the total flow rate) at low C_2H_6 conversions, as shown in Figure S1.

10.1002/cctc.201901585

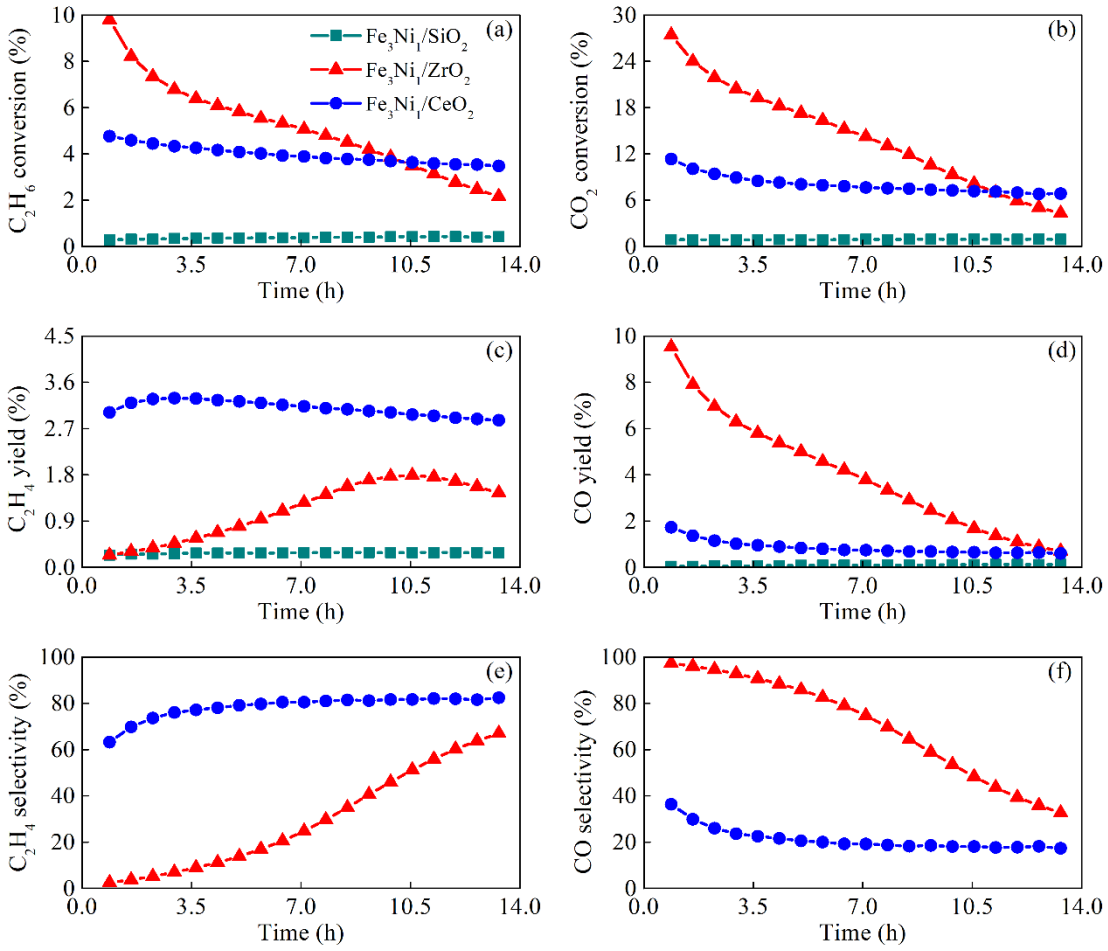

Figure 1. Conversion of (a) C_2H_6 and (b) CO_2, yield of (c) C_2H_4 and (d) CO, and selectivity toward (e) CH_4 and (f) CO over Fe_3Ni_1/SiO_2, Fe_3Ni_1/ZrO_2, and Fe_3Ni_1/CeO_2 plotted versus time on stream for reaction of C_2H_6 and CO_2 (10 mL/min C_2H_6 + 10 mL/min CO_2 + 20 mL/min Ar, 100 mg catalyst) at 873 K.

10.1002/cctc.201901585

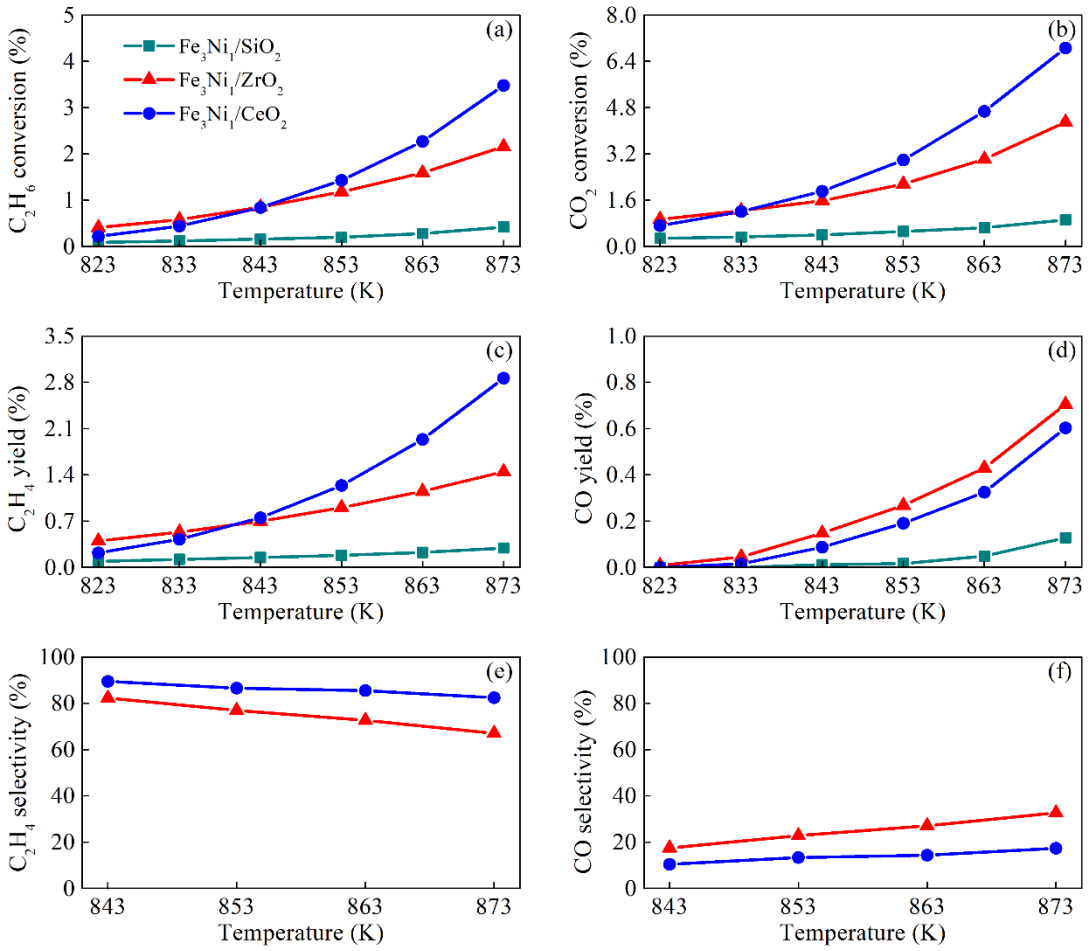

Figure 2. Conversion of (a) C_2H_6 and (b) CO_2, yield of (c) C_2H_4 and (d) CO, and selectivity toward (e) CH_4 and (f) CO over Fe_3Ni_1/SiO_2, Fe_3Ni_1/ZrO_2, and Fe_3Ni_1/CeO_2 for reaction of C_2H_6 and CO_2 (10 mL/min C_2H_6 + 10 mL/min CO_2 + 20 mL/min Ar, 100 mg catalyst) at different temperatures with 10 K temperature increment.

Table 1 Summary of flow reactor results for CO_2 + C_2H_6 reaction (10 ml/min CO_2 + 10 ml/min C_2H_6 + 20 ml/min Ar) at 873 K. Values of conversion, yield, selectivity, TOF and STY calculated by averaging data points between 11-13 h on stream

Catalyst	Conversion, %		Yield, %		Selectivity, %		TOF_1, time/site/min		TOF_2, mol/mol$_{Ni}$/min		STY, μmol/g_{cat}/min	
	C_2H_6	CO_2	C_2H_4	CO	C_2H_4	CO	C_2H_6	CO_2	C_2H_6	CO_2	C_2H_4	CO
Fe_3Ni_1/SiO_2	0.4	0.9	0.3	0.1	-	-	-	-	0.2	0.5	13.9	57.9
Fe_3Ni_1/ZrO_2	2.6	5.6	1.6	1.0	61.7	37.9	3.5	7.5	1.3	2.7	63.6	310.3
Fe_3Ni_1/CeO_2	3.5	6.9	2.9	0.6	82.0	17.8	2.7	5.2	1.7	3.3	116.8	346.1
$Fe_{0.75}Ni_{0.25}/CeO_2$	2.2	4.7	1.7	0.5	76.7	23.0	1.9	4.1	4.2	9.0	71.8	246.3
$Fe_{1.5}Ni_{0.5}/CeO_2$	3.1	6.2	2.5	0.6	79.2	20.5	2.6	5.1	3.0	5.9	101.0	316.2
Fe_6Ni_2/CeO_2	3.4	8.7	2.3	1.1	67.4	32.3	2.6	6.7	0.8	2.1	92.6	465.2
$Fe_{12}Ni_4/CeO_2$	3.5	13.1	1.1	2.4	31.9	67.7	2.1	8.1	0.4	1.6	45.3	762.8

Effect of metal loading amount

Time-on-stream catalytic activities of the CeO_2-supported $Fe_{3x}Ni_x$ (x = 0.25, 0.5, 1, 2, and 4) catalysts with different metal loadings are shown in Figure 3. The steady-state conversion, yield, selectivity, turnover frequency (TOF) and space-time yield (STY) are also listed in Table 1. When the loading amounts of the active metals (i.e., Fe and Ni) are low, the C_2H_6 conversion monotonically increases while the C_2H_4 selectivity remains stable (80%) with the increase in the loading amount. However, if the amount of loaded Fe (Ni) exceeds 1.4 (0.5) wt%, the conversion of C_2H_6 remains stable but the dominant pathway transforms from favoring the oxidative dehydrogenation reaction (e.g., Fe_3Ni_1/CeO_2) to favoring the dry reforming reaction (e.g., $Fe_{12}Ni_4/CeO_2$), greatly lowering the C_2H_4 selectivity (from 82% to 32%). The maximum C_2H_4 yield is observed on Fe_3Ni_1/CeO_2 with 1.4 wt% Fe and 0.5 wt% Ni. The conversion, yield, and selectivity over the CeO_2-supported $Fe_{3x}Ni_x$ (x = 0.25, 0.5, 1, 2, and 4) catalysts at different temperatures varying from 873 K to 823 K after 13 h operation are compared in Figure 4. For Fe_3Ni_1/CeO_2 and $Fe_{12}Ni_4/CeO_2$, the conversion of C_2H_6 and CO_2, and the yield of C_2H_4 and CO gradually increase with increasing temperature while the selectivity of C_2H_4 and CO remains nearly constant.

10.1002/cctc.201901585

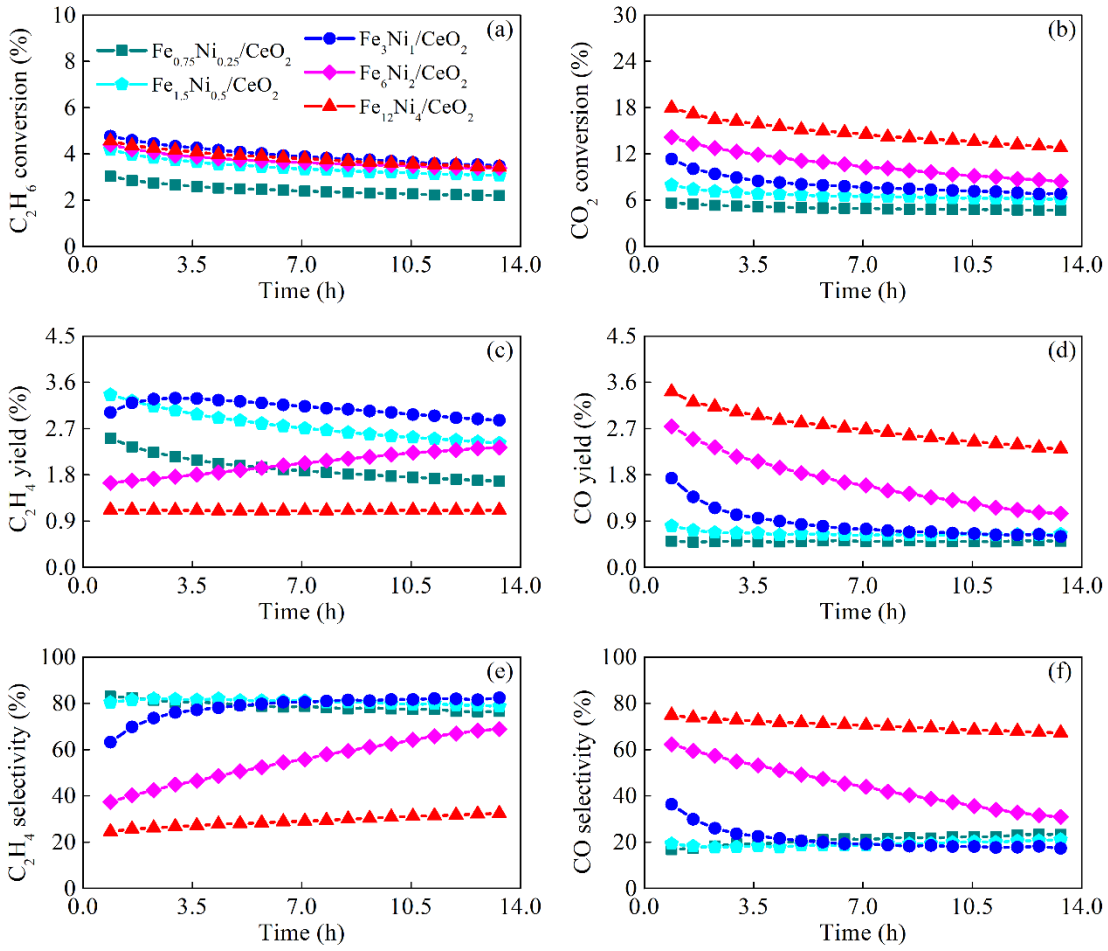

Figure 3. Conversion of (a) C_2H_6 and (b) CO_2, yield of (c) C_2H_4 and (d) CO, and selectivity toward (e) CH_4 and (f) CO over CeO_2-supported $Fe_{3x}Ni_x$ (x = 0.25, 0.5, 1, 2, and 4) catalysts plotted versus time on stream for reaction of C_2H_6 and CO_2 (10 mL/min C_2H_6 + 10 mL/min CO_2 + 20 mL/min Ar, 100 mg catalyst) at 873 K.

10.1002/cctc.201901585

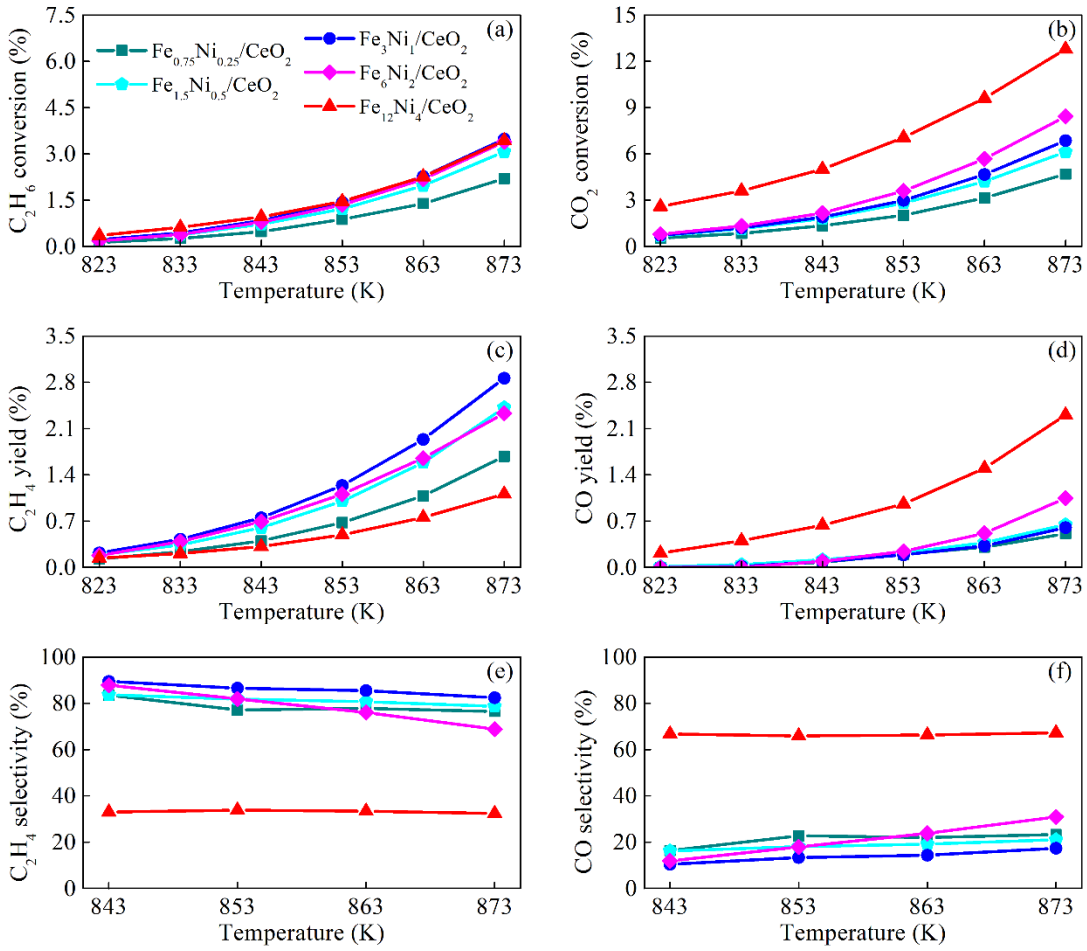

Figure 4. Conversion of (a) C_2H_6 and (b) CO_2, yield of (c) C_2H_4 and (d) CO, and selectivity toward (e) CH_4 and (f) CO over CeO_2-supported $Fe_{3x}Ni_x$ (x = 0.25, 0.5, 1, 2, and 4) catalysts for reaction of C_2H_6 and CO_2 (10 mL/min C_2H_6 + 10 mL/min CO_2 + 20 mL/min Ar, 100 mg catalyst) at different temperatures with 10 K temperature increment.

Ex-situ and in-situ X-ray diffraction (XRD) characterization

The structures of the fresh and spent $Fe_{12}Ni_4/CeO_2$, Fe_6Ni_2/CeO_2, Fe_3Ni_1/CeO_2, and Fe_3Ni_1/ZrO_2 catalysts were investigated using *ex-situ* XRD. As shown in Figure 5, the XRD patterns exhibit the typical diffraction peaks of CeO_2 with a cubic fluorite structure and ZrO_2 with a monoclinic crystalline structure. The crystalline sizes of CeO_2 and ZrO_2 are estimated about 33 nm and 14 nm, respectively, based on the XRD peak width. XRD peaks of NiO are not observed in the fresh samples, indicating that NiO is well dispersed on both support with relatively small crystallite sizes. When the loading amount of Fe exceeds 2.9 wt%, crystalline Fe_3O_4 or Fe_2O_3 are observed in the fresh CeO_2-supported $Fe_{3x}Ni_x$ catalysts with weak (311), (400) and (440) reflections at 5.45 °, 6.58 °and 9.31 °, respectively. After over 13 h reaction at 873 K, the diffraction intensity of crystalline Fe_3O_4 or Fe_2O_3 becomes stronger and the corresponding peak width gets narrower, indicating that the crystal size is increased. Weak peaks at 4.65˚ and 5.70˚, which are attributed to the (220) and (222) reflections of crystalline Fe_3O_4 or Fe_2O_3, are also observed. New diffraction peaks at 6.75˚ and 7.79˚ appear in the XRD patterns for the spent CeO_2-support FeNi catalysts, implying that metallic Ni (or Ni-rich NiFe alloy) is formed under reaction conditions.

10.1002/cctc.201901585

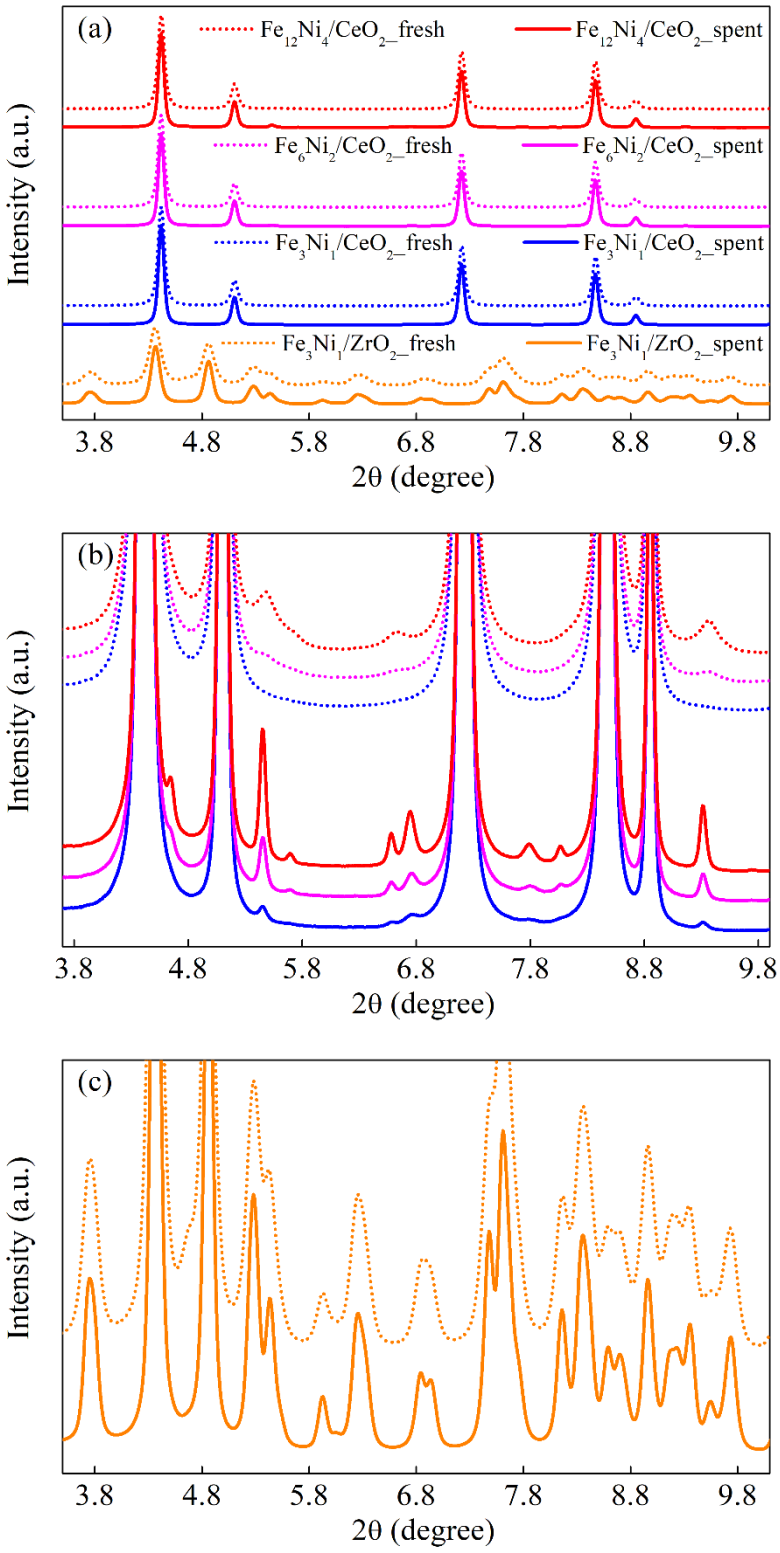

Figure 5. *Ex-situ* XRD profiles of the fresh and spent $Fe_{12}Ni_4/CeO_2$, Fe_6Ni_2/CeO_2, Fe_3Ni_1/CeO_2, and Fe_3Ni_1/ZrO_2 catalysts in the 2θ range of 3.8˚ to 9.8˚.

The structural evolution of $Fe_{12}Ni_4/CeO_2$, Fe_6Ni_2/CeO_2, Fe_3Ni_1/CeO_2, and Fe_3Ni_1/ZrO_2 under reaction conditions was examined using *in-situ* XRD measurements. Figure S2 and Figure 6 show the variation of diffraction peaks in different 2θ ranges with time for the four catalysts. For CeO_2-supported FeNi catalysts under reaction conditions, the diffraction peaks at 5.42°, 5.65°, 6.54°, 8.02°, and 9.25° are assigned to the (311), (222), (400), (422) and (440) reflections of crystalline Fe_3O_4 or Fe_2O_3, respectively. According to a previous work [2], the (111) and (200) reflections of metallic Ni with the FCC (face-centered cubic) structure are located at 6.74 °and 7.77 °, based on which the calculated lattice constant was 3.558 Å, slightly larger than the value of 3.524 Å for bulk Ni due to thermal expansion. Compared to metallic Ni, the diffraction peaks of the reduced metal on CeO_2-supported $Fe_{3x}Ni_x$ catalysts under reaction conditions are slightly shifted to lower 2θ values with a calculated lattice constant of 3.570 Å. The larger cell parameter suggests that Ni particles are alloyed with Fe (FCC structure), thus the peaks at 6.71° and 7.75° are assigned to the (111) and (200) reflections of Ni-rich NiFe alloy. For CeO_2-supported $Fe_{3x}Ni_x$ catalysts, the diffraction peak centered at 7.75° under reaction conditions slightly shifts to 7.77° under CO_2 treatment conditions as shown in Figures S3-S5 with the calculated lattice constant of 3.561 Å (more close to metallic Ni 3.558 Å), indicating that the Fe species in Ni-rich NiFe alloy formed under reaction conditions can be re-oxidized in a CO_2/He flow to form an amorphous FeO_x thin layer [31]. The peak intensities of crystalline Fe_3O_4 or Fe_2O_3 and metallic NiFe alloy increase when increasing the metal loading amount. Based on the evolution of the peaks centered at 6.71°, it can be concluded that

the growth of metallic NiFe crystal particles starts at a temperature of 833 K in the presence of reactants (2.5 mL/min C_2H_6 + 2.5 mL/min CO_2 + 5.0 mL/min He). The intensity and position of this peak do not change after 10-minute reaction, indicating that the formed metallic NiFe alloy particles are relatively stable under reaction conditions. The diffraction peaks of crystalline Fe_3O_4 or Fe_2O_3 and metallic Ni (or Ni-rich NiFe alloy) are barely observed over Fe_3Ni_1/ZrO_2, suggesting that both Fe and Ni species are highly dispersed on ZrO_2 under reaction conditions.

10.1002/cctc.201901585

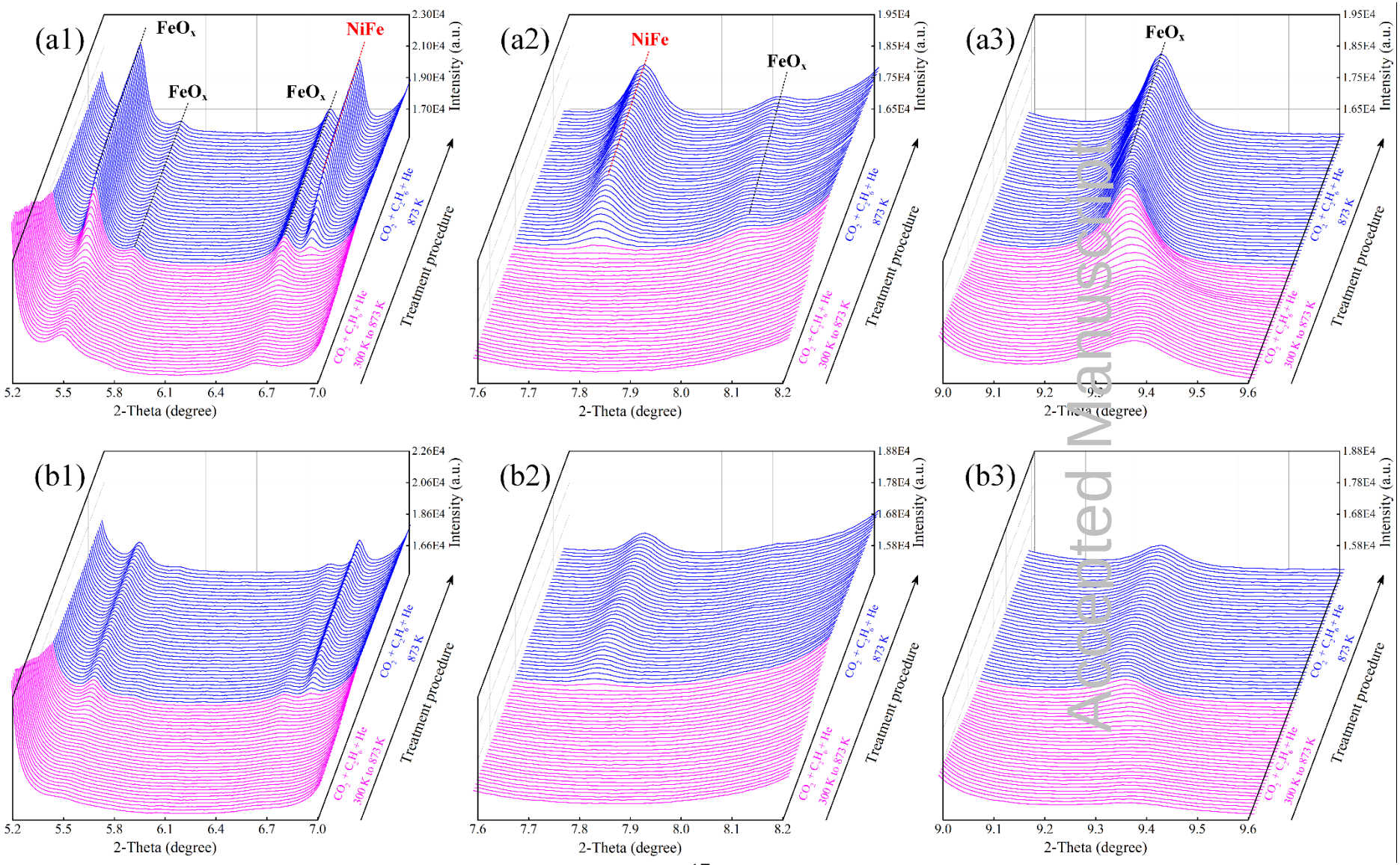

10.1002/cctc.201901585

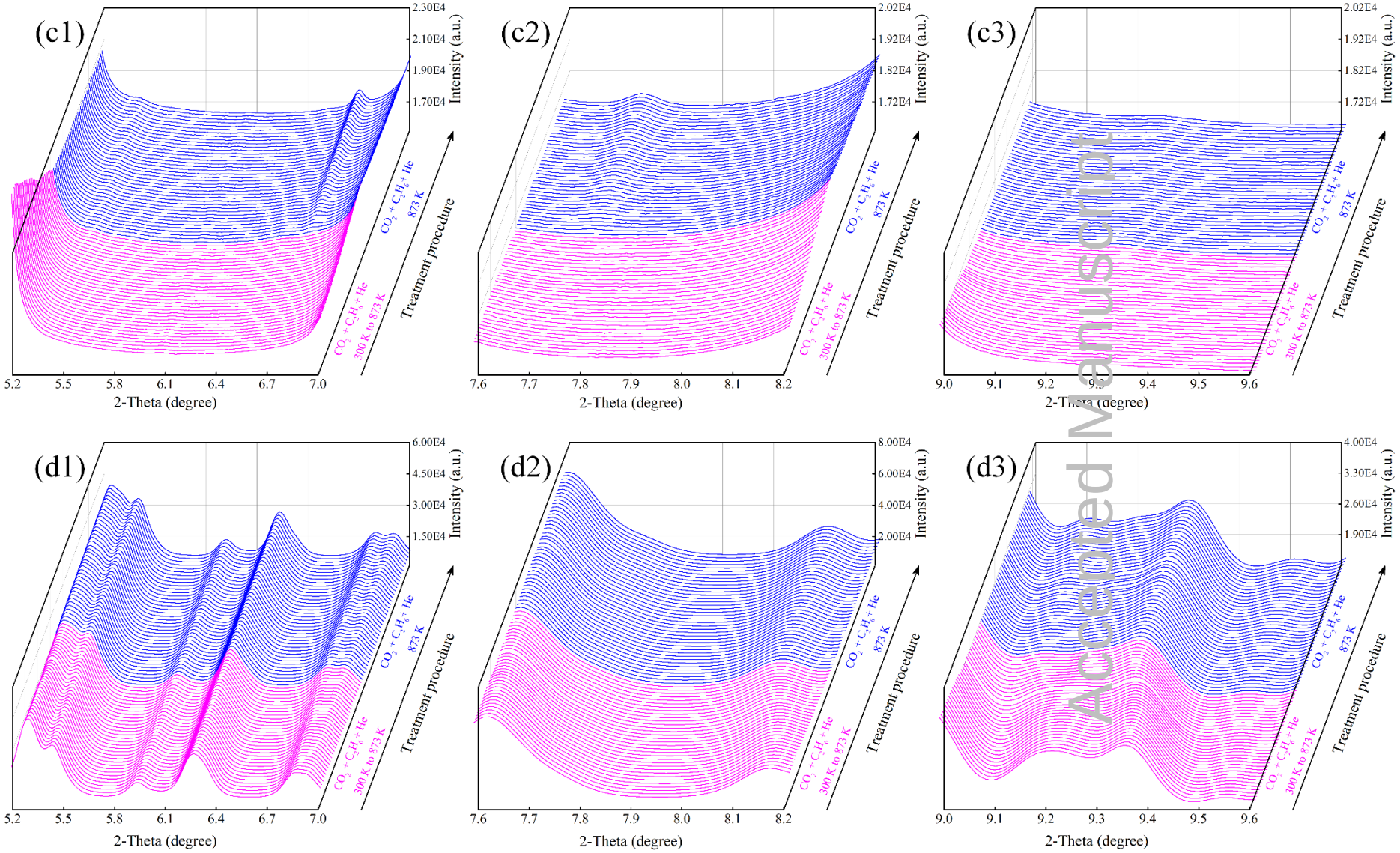

Figure 6. Evolution of the *in-situ* XRD profiles under various conditions: (a) $Fe_{12}Ni_4/CeO_2$, (b) Fe_6Ni_2/CeO_2, (c) Fe_3Ni_1/CeO_2, and (d) Fe_3Ni_1/ZrO_2 in the 2θ range of (1) 5.2˚ to 7.0˚, (2) 7.6˚ to 8.2˚, and (3) 9.0˚ to 9.6˚. Magenta line, temperature ramping stage: from 300 K to 873 K, 2.5 mL/min C_2H_6 + 2.5 mL/min CO_2 + 5.0 mL/min He, 10 mg catalyst; blue line, reaction conditions: 873 K, 2.5 mL/min C_2H_6 + 2.5 mL/min CO_2 + 5.0 mL/min He.

In-situ X-ray absorption fine structure (XAFS) measurements

In order to further determine the oxidation state of Ni and Fe on Fe_3Ni_1/ZrO_2, Fe_3Ni_1/CeO_2, and $Fe_{12}Ni_4/CeO_2$ under reaction conditions, *in-situ* X-ray absorption near edge structure (XANES) spectra were collected, as shown in Figure 7. Based on the Ni K-edge XANES spectra, the Ni species in all three fresh catalysts show similar near edge features as the standard NiO. The Fe-K edge XANES spectra suggest that the Fe species in all fresh samples exhibit near edge features between Fe_3O_4 and Fe_2O_3. For all three catalysts under reaction conditions, the oxidation state of Ni is metallic and the Fe species are also reduced and show near edge features between FeO and Fe_3O_4. The detailed EXAFS fittings of the Ni and Fe K-edge spectra of Fe_3Ni_1/ZrO_2, Fe_3Ni_1/CeO_2, and $Fe_{12}Ni_4/CeO_2$ under reaction conditions are summarized in Table 2, Table 3, Figures S6 and S7. The EXAFS fitting results reveal that the coordination numbers (CNs) of Ni-Ni(Fe) on the three catalysts under reaction conditions are 9.8, 9.8 and 11.3, respectively, indicating that the Ni-rich NiFe alloy resides in the form of particles with diameters of 2.2-4.0 nm (based on hemisphere FCC models). According to the EXAFS fitting results of the Fe K-edge spectra, the total CNs of Fe-O-Fe (2.88 Å and 3.07 Å) in $Fe_{12}Ni_4/CeO_2$ are 3.6. The Fe-Fe(Ni) coordination (2.50 Å) is observed in $Fe_{12}Ni_4/CeO_2$, indicating that there is a part of Fe species in the form of metallic Fe. This conclusion is consistent with the formation of Ni-rich NiFe alloy with the FCC structure revealed by XRD results as the XRD peaks of metallic Fe with the BCC (body-centered cubic) structure are not observed. In contrast, all the Fe species in the Fe_3Ni_1/CeO_2 catalyst are oxidized and the total CNs of Fe-O-Fe (2.85 Å and 3.04 Å) is

also slightly reduced to only 2.8. The CNs of Fe-O-Fe (2.95 Å and 3.34 Å) on Fe_3Ni_1/ZrO_2 are fairly low (0.9 for each), suggesting that Fe oxides might be highly dispersed on Fe_3Ni_1/ZrO_2. The bond lengths of both Fe-O-Fe shells expand, indicating that the ZrO_2 support may influence the geometry of supported Fe species.

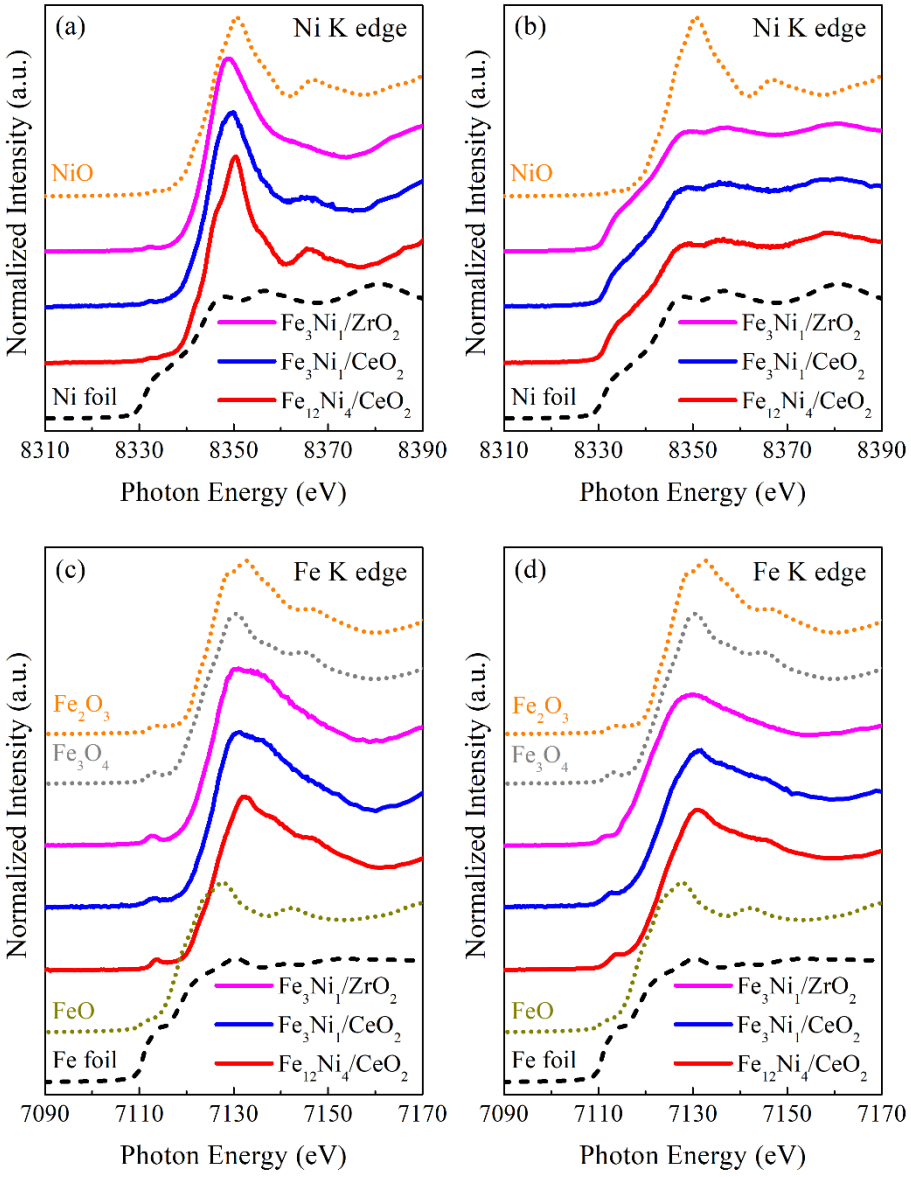

Figure 7 *In-situ* XANES spectra: (a) Ni K-edge of fresh Fe_3Ni_1/ZrO_2, Fe_3Ni_1/CeO_2, and $Fe_{12}Ni_4/CeO_2$ with Ni foil and NiO as references; (b) Ni K-edge of Fe_3Ni_1/ZrO_2, Fe_3Ni_1/CeO_2, and $Fe_{12}Ni_4/CeO_2$ under reaction conditions with Ni foil and NiO as

references; (c) Fe K-edge of fresh Fe_3Ni_1/ZrO_2, Fe_3Ni_1/CeO_2, and $Fe_{12}Ni_4/CeO_2$ with Fe foil, FeO, Fe_3O_4 and Fe_2O_3 as references; (d) Fe K-edge of Fe_3Ni_1/ZrO_2, Fe_3Ni_1/CeO_2, and $Fe_{12}Ni_4/CeO_2$ under reaction conditions with Fe foil, FeO, Fe_3O_4 and Fe_2O_3 as references. Reaction conditions: 873 K, 5 mL/min C_2H_6 + 5 mL/min CO_2 + 10 mL/min He, 100 mg catalyst.

Table 2 Ni K-edge EXAFS fitting results of Fe_3Ni_1/ZrO_2, Fe_3Ni_1/CeO_2 and $Fe_{12}Ni_4/CeO_2$ under reaction conditions (5 mL/min C_2H_6 + 5 mL/min CO_2 + 10 mL/min He, 100 mg catalyst, 873 K)

Sample	Shell	Bond length (Å)	CN	σ^2 (Å^2)	E_0 shift (eV)
Fe_3Ni_1/ZrO_2	Ni-Ni(Fe)	2.47 ± 0.01	9.8 ± 0.9	0.016 ± 0.001	2.9
Fe_3Ni_1/CeO_2	Ni-Ni(Fe)	2.47 ± 0.03	9.8 ± 1.2	0.018 ± 0.001	1.3
$Fe_{12}Ni_4/CeO_2$	Ni-Ni(Fe)	2.47 ± 0.01	11.3 ± 1.4	0.019 ± 0.001	-9.8

Table 3 Fe K-edge EXAFS fitting results of Fe_3Ni_1/ZrO_2, Fe_3Ni_1/CeO_2 and $Fe_{12}Ni_4/CeO_2$ under reaction conditions (5 mL/min C_2H_6 + 5 mL/min CO_2 + 10 mL/min He, 100 mg catalyst, 873 K)

Sample	Shell	Bond length (Å)	CN	σ^2 (Å^2)	E_0 shift (eV)
Fe_3Ni_1/ZrO_2	Fe-O	1.93 ± 0.02	3.9 ± 0.4	0.010 ± 0.001	-4.6
	Fe-O-Fe(Ni)	2.95 ± 0.03	0.9 ± 0.3	0.012 ± 0.001	

	Fe-O-Fe(Ni)	3.34 ±0.03	0.9 ±0.3	0.012 ±0.001	
Fe_3Ni_1/CeO_2	Fe-O	1.92 ±0.03	3.0 ±0.3	0.013 ±0.001	-9.1
	Fe-O-Fe(Ni)	2.85 ±0.04	1.0 ±0.5	0.012 ±0.001	
	Fe-O-Fe(Ni)	3.06 ±0.04	1.8 ±0.6	0.012 ±0.001	
$Fe_{12}Ni_4/CeO_2$	Fe-O	1.96 ±0.03	3.9 ±0.3	0.009 ±0.001	-1.9
	Fe-Fe(Ni)	2.50 ±0.03	0.9 ±0.3	0.010 ±0.001	
	Fe-O-Fe	2.88 ±0.04	1.8 ±0.4	0.010 ±0.001	
	Fe-O-Fe	3.07 ±0.04	1.8 ±0.3	0.010 ±0.001	

Discussion of active sites

As shown in Figure 1 and Table 1, the supported-Fe_3Ni_1 catalysts with different oxide supports present distinguishable catalytic activity. As an inert and irreducible support, SiO_2 cannot promote the activation of CO_2 via direct C=O bond scission, which is very different from the reducible supports (e.g. CeO_2). Therefore, Fe_3Ni_1/SiO_2 shows little activity for either the oxidative dehydrogenation or dry reforming of ethane. Fe_3Ni_1/ZrO_2 shows high initial activity and selectivity for dry reforming of ethane but accompanied by severe deactivation. Fe_3Ni_1/CeO_2 exhibits excellent activity and selectivity for oxidative dehydrogenation of ethane.

According to the previous work [2], the Ni-CeO_x interfaces are identified as the most likely active sites for dry reforming of ethane with CO_2 (efficient C-C bond scission to produce synthesis gas), while the Ni-FeO_x/CeO_x interfaces are identified as the most likely active sites for CO_2-assisted dehydrogenation of ethane (selective C-H

bond cleavage to produce ethylene). The oxygen species for dry reforming at the Ni-CeO_x interfacial sites might mainly come from the Ce(III)/Ce(IV) redox couple while the oxygen species for oxidative dehydrogenation at the Ni-FeO_x/CeO_x interfacial sites might be originated from the Fe(II)/Fe(III) redox couple. For Fe_3Ni_1/ZrO_2, Ni is in a state of metallic nickel (Ni^0) while Fe exists in the form of oxides (FeO_x, shows near edge features between FeO and Fe_3O_4) under reaction conditions (Figure 7). However, the CNs of Fe-O-Fe on Fe_3Ni_1/ZrO_2 are fairly low (Table 3) and the diffraction peaks of any Ni^0 or FeO_x species are not observed on Fe_3Ni_1/ZrO_2 under reaction conditions (Figure 6), indicating that both the Ni^0 and FeO_x species distribute relatively sparsely and evenly over the ZrO_2 support. Therefore, the Ni-ZrO_2 interfacial sites likely dominate the conversion of ethane with CO_2, exhibiting a high initial CO selectivity (over 95%). According to the thermogravimetric analysis (TGA) results (Figure S8), the deactivation of Fe_3Ni_1/ZrO_2 is suggested to be mainly caused by coking on the surface. As the Ni-ZrO_2 interfacial sites are gradually covered by the coke during the reaction, the C_2H_4 selectivity continuously increases during the course of reaction, as shown in Figure 1.

For CeO_2-supported $Fe_{3x}Ni_x$ (x = 0.25, 0.5, 1, 2, 4) catalysts, when the loading amount of Fe (Ni) is lower than 1.4 (0.5) wt%, the Ni-rich NiFe alloy exists as small particles (based on the *in-situ* XRD and XAFS measurements); the FeO_x species prefer to exist underneath the predominantly Ni particles, likely forming the Ni-FeO_x/CeO_x interfacial sites that are identified as the most likely active sites for CO_2-assisted dehydrogenation of ethane [2]. More Ni-FeO_x/CeO_x interfacial sites are formed with

the increase of metal loading, leading to higher activity for CO_2-assisted oxidative dehydrogenation of ethane with over 80% ethylene selectivity. When the loading amount of Fe (Ni) exceeds 5.7 (2.0) wt%, the Ni-rich NiFe alloy resides as lager particles with diameters of 4.0 nm. The metallic Fe-Fe(Ni) bonding at 2.50Å is only found on $Fe_{12}Ni_4/CeO_2$ while barely seen on Fe_3Ni_1/CeO_2 (Table 3), suggesting that the ratio of metallic Fe in overall Fe species on $Fe_{12}Ni_4/CeO_2$ is much higher than that on Fe_3Ni_1/CeO_2. This means that FeO_x on the perimeter of Ni particles on $Fe_{12}Ni_4/CeO_2$ is likely reduced. Therefore, the NiFe-CeO_x interfacial sites that favor the dry reforming pathway via efficient C-C bond scission to produce synthesis gas are likely formed on $Fe_{12}Ni_4/CeO_2$, leading to a corresponding decrease in ethylene selectivity (from 82% over Fe_3Ni_1/CeO_2 to 32% over $Fe_{12}Ni_4/CeO_2$).

Conclusions

The *in-situ* XRD and XAFS characterization was combined with flow reactor evolution to identify the oxidation state and the dispersion of Ni and Fe species on FeNi-based catalysts for CO_2-assisted oxidative dehydrogenation of ethane, aiming to gain a better understanding of the role of the oxide support and the metal loading amount in tuning the catalytic activity and selectivity. The formation of Ni-rich NiFe alloy with the FCC structure and crystalline Fe_3O_4 or Fe_2O_3 on CeO_2-supported $Fe_{3x}Ni_x$ catalysts under reaction conditions was revealed by the *in-situ* XRD and XAFS measurements. Among these FeNi-based catalysts, Fe_3Ni_1/CeO_2 exhibits the best catalytic activity and ethylene selectivity. The increased CO selectivity through the dry reforming pathway

observed on Fe_3Ni_1/ZrO_2 and $Fe_{12}Ni_4/CeO_2$ is likely due to the formation of Ni-ZrO_2 and NiFe-CeO_x interfacial sites, respectively. The ideal oxidative dehydrogenation catalyst requires a reducible oxide (CeO_2) to facilitate the activation of CO_2 via direct C=O bond scission and optimal loading amounts of active metals (Fe and Ni) to form the active sites (Ni-FeO_x/CeO_x interfacial sites) for CO_2-assisted dehydrogenation of ethane via the selective C-H bond cleavage to produce ethylene.

Experimental Section

Catalyst preparation

The supported FeNi catalysts were synthesized by wetness co-impregnation over commercial supports with an aqueous solution of the respective metal precursors. $Ni(NO_3)_2{\cdot}6H_2O$ (Sigma-Aldrich, 99.999% trace metals basis), $Fe(NO_3)_3{\cdot}9H_2O$ (Sigma-Aldrich, 99.999% trace metals basis), SiO_2 (Alfa Aesar, pellets, 250 m^2/g), ZrO_2 (Alfa Aesar, pellets, 90 m^2/g) and CeO_2 (Sigma-Aldrich, nanopowder, 35-45 m^2/g) were used. After impregnation, the catalysts were dried at 363 K for 12 h, then ramped to 723 K with a rate of 0.8 K/min and calcined for 4 h in air. The metal loading amounts (and atomic ratio as well) for these catalysts are listed in Table S1.

Catalyst characterization

The pulse CO chemisorption experiments were carried out in an Altamira AMI-300 ip system to obtain the CO uptake value for each catalyst. 100 mg of fresh catalyst was firstly reduced at 873 K for 30 min using a mixture of 10% H_2 in Ar (30 ml/min),

then purged with He (50 ml/min) for degassing and cooled down to 313 K. Pulses of 10% CO in He (590 μL loop) were injected into the He stream until the peak area became constant. The amount of CO flowing out of the reactor was monitored by a thermal conductivity detector (TCD). The CO uptake offers an approach to estimate the turnover frequency (TOF) of each catalyst. The CO uptake values for the fresh catalysts are also listed in Table S1.

The temperature-programmed reduction (TPR) experiments were carried out in the same Altamira AMI-300 ip instrument. 50 mg of fresh catalyst was pre-treated with a He flow (30 ml/min) at 393 K for 30 min. After cooled down to 303 K, the TPR measurement was performed with a heating rate of 10 K/min to 873 K, using a mixture of 10% H_2 in Ar with a constant flow rate of 50 ml/min. The variation of hydrogen consumption with reduction temperature was continuously recorded by a TCD.

The *ex-situ* and *in-situ* X-ray diffraction (XRD) patterns for Fe_3Ni_1/ZrO_2, Fe_3Ni_1/CeO_2, Fe_6Ni_2/CeO_2, and $Fe_{12}Ni_4/CeO_2$ were collected at beamline 17-BM of advanced photon source (APS) at Argonne National Lab (ANL). The X-ray wavelength was 0.24128 Å. 10 mg of sieved catalyst (60-80 mesh) was loaded into a quartz capillary with two open ends (1.0 mm OD, 0.9 mm ID and 75 mm in length), packed by quartz wools at both sides of the sample. The sample was heated to 873 K at a rate of 20 K/min and held at 873 K for 40 min in the presence of reactants (2.5 mL/min C_2H_6 + 2.5 mL/min CO_2 + 5.0 mL/min He). Before ramped down to room temperature, the sample was treated in a CO_2/He flow (2.5 mL/min CO_2 + 7.5 mL/min He) for 30 min and then in a H_2/He flow (5.0 mL/min H_2 + 5.0 mL/min He) for 30 min. Two-

dimensional XRD images were continuously collected by a PerkinElmer a-Si flat panel detector. The images were subsequently processed with GSAS-II to obtain XRD profiles, and Rietveld refinement was performed to extract structural information.

The *in-situ* Ni K-edge (8333 eV) and Fe K-edge (7112 eV) X-ray absorption fine structure (XAFS) spectra for Fe_3Ni_1/ZrO_2, Fe_3Ni_1/CeO_2, and $Fe_{12}Ni_4/CeO_2$ were collected at Beamline 9-BM of Advanced Photon Source (APS) at Argonne National Laboratory (ANL). For each run, 100 mg sample (60-80 mesh) was loaded into a home-designed *in-situ* micro-channel reactor with graphite paper as the window material. Measurements were performed in a fluorescence mode using a vortex detector. The sample was firstly reduced in a H_2/He flow (10 mL/min H_2 + 10 mL/min He) at 723 K for 60 min. The flow was the switched to a mixture of reactants (5 mL/min C_2H_6 + 5 mL/min CO_2 + 10 mL/min He), and the sample was heated to 873 K at a rate of 10 K/min and held for 30 min. The spectra were collected under reaction conditions and then analyzed using IFEFFIT package. Ni foil, NiO, Fe foil, FeO, Fe_3O_4, and Fe_2O_3 were employed as references of EXAFS fitting.

Catalyst evaluation

Flow reactor studies of C_2H_6 + CO_2 reactions over supported FeNi catalysts were performed in a quartz tube reactor under atmospheric pressure. For steady-state experiments, 100 mg of sieved catalyst (40-60 mesh) was used. The catalyst was firstly reduced under a H_2/Ar mixture (20 mL/min H_2 + 20 mL/min Ar) at 723 K for one hour prior to reaction. After reduction, the temperature was increased at a rate of 10 K/min

and held at 873 K in the presence of reactants (10 mL/min C_2H_6 + 10 mL/min CO_2 + 20 mL/min Ar) for at least 13 hours. Then, the temperature was changed from 873 K to 823 K with 10 K increments to study the effect of temperature on the reaction rates of C_2H_6 and CO_2. The concentrations of gas products were analyzed on-line by a gas chromatography instrument (Agilent 7890B) equipped with a flame ionization detector (FID) and a TCD. Blank experiments were carried out at 873 K using a blank quartz tube. Little activity was found, indicating that the quartz tube and the gas-phase reaction have no significant effect on the reaction.

The steady state conversion (X), C_2H_6 based yield (Y), C_2H_6 based selectivity (S), turnover frequency (TOF) and space-time yield (STY) were defined as

$$X_{\text{reactant}} = \frac{F_{\text{reactant}}^{\text{inlet}} - F_{\text{reactant}}^{\text{outlet}}}{F_{\text{reactant}}^{\text{inlet}}} \quad (1)$$

$$Y_{C_2H_4} = \frac{F_{C_2H_4}^{\text{outlet}}}{F_{C_2H_6}^{\text{inlet}}} \quad (2)$$

$$Y_{\text{CO}} = \frac{F_{\text{CO originated from } C_2H_6}^{\text{outlet}}}{2 \times F_{C_2H_6}^{\text{inlet}}} \quad (3)$$

Here, the amount of CO produced for C_2H_6 can be calculated based on the oxygen balance,

$$F_{\text{CO originated from } C_2H_6}^{\text{outlet}} = F_{\text{CO}}^{\text{outlet}} - \left(\frac{F_{\text{CO}}^{\text{outlet}} + F_{H_2O}^{\text{outlet}}}{2} \right) \quad (4)$$

$$S_{C_2H_4} = \frac{Y_{C_2H_4}}{X_{C_2H_6}} \quad (5)$$

$$S_{\text{CO}} = \frac{Y_{\text{CO}}}{X_{C_2H_6}} \quad (6)$$

$$TOF_1 = \frac{F_{\text{reactant}}^{\text{inlet}} \times X}{U_{\text{CO}} \times W_{\text{catalyst}}}, \quad \text{time/site/min} \tag{7}$$

$$TOF_2 = \frac{F_{\text{reactant}}^{\text{inlet}} \times X}{L_{\text{Ni}} \times W_{\text{catalyst}}}, \quad \text{mol/mol}_{\text{Ni}}\text{/min} \tag{8}$$

$$STY_{\text{product}} = \frac{F_{\text{product}}^{\text{outlet}}}{W_{\text{catalyst}}}, \quad \mu\text{mol/}g_{\text{catalyst}}\text{/min} \tag{9}$$

where, F is the flow rate of reactant, mol/min; U_{CO} is the CO uptake value, μmol CO/g; W is the weight of catalyst used, g; L_{Ni} is the loading amount of Ni, μmol Ni/g.

Acknowledgments

The work is sponsored by the U.S. Department of Energy (DOE), Office of Basic Energy Sciences, Catalysis Science Program, under Contract No. DE-SC0012704. The *in-situ* XRD/XAFS measurements were performed at the 17-BM/9-BM beamline of the Advanced Photon Source (APS) at Argonne National Laboratory (DE-AC02-06CH11357).

References

[1] E. Gomez, B. Yan, S. Kattel, J. G. Chen, *Nat. Rev. Chem.* **2019**, DOI: 10.1038/s41570-41019-40128-41579.

[2] B. Yan, S. Yao, S. Kattel, Q. Wu, Z. Xie, E. Gomez, P. Liu, D. Su, J. G. Chen, *Proc. Natl. Acad. Sci. U. S. A.* **2018,** *115*, 8278.

[3] T.-Q. Lei, Y.-H. Cheng, C.-X. Miao, W.-M. Hua, Y.-H. Yue, Z. Gao, *Fuel Process. Technol.* **2018,** *177*, 246-254.

[4] A. Talati, M. Haghighi, F. Rahmani, *Adv. Powder Technol.* **2016,** *27*, 1195-1206.

[5] D. Mukherjee, S.-E. Park, B. M. Reddy, *J. CO2 Util.* **2016,** *16*, 301-312.

[6] F. Rahmani, M. Haghighi, M. Amini, *J. Ind. Eng. Chem.* **2015,** *31*, 142-155.

[7] B. H. Yan, X. F. Yang, S. Y. Yao, J. Wan, M. Myint, E. Gomez, Z. H. Xie, S. Kattel, W. Q. Xu, J. G. G. Chen, *ACS Catal.* **2016,** *6*, 7283-7292.

[8] B. H. Zhao, B. H. Yan, S. Y. Yao, Z. H. Xie, Q. Y. Wu, R. Ran, D. Weng, C. Zhang, J. G. G. Chen, *J. Catal.* **2018,** *358*, 168-178.

[9] S. Kattel, J. G. Chen, P. Liu, *Catal. Sci. Technol.* **2018,** *8*, 3748-3758.

[10] Z. Shen, J. Liu, H. Xu, Y. Yue, W. Hua, W. Shen, *Appl. Catal. A* **2009,** *356*, 148-153.

[11] R. Koirala, R. Buechel, F. Krumeich, S. E. Pratsinis, A. Baiker, *ACS Catal.* **2015,** *5*, 690-702.

[12] E. Asghari, M. Haghighi, F. Rahmani, *J. Mol. Catal. A: Chem.* **2016,** *418-419*, 115-124.

[13] N. Mimura, I. Takahara, M. Inaba, M. Okamoto, K. Murata, *Catal. Commun.* **2002,** *3*, 257-262.

[14] N. Mimura, M. Okamoto, H. Yamashita, S. T. Oyama, K. Murata, *J. Phys. Chem. B* **2006,** *110*, 21764-21770.

[15] S. Deng, H. Li, S. Li, Y. Zhang, *J. Mol. Catal. A: Chem.* **2007,** *268*, 169-175.

[16] S. Deng, S. Li, H. Li, Y. Zhang, *Ind. Eng. Chem. Res.* **2009,** *48*, 7561-7566.

[17] X. Zhang, Q. Ye, B. Xu, D. He, *Catal. Lett.* **2007,** *117*, 140-145.

[18] R. Koirala, R. Buechel, S. E. Pratsinis, A. Baiker, *Appl. Catal. A* **2016,** *527*, 96-108.

[19] M. D. Porosoff, M. N. Z. Myint, S. Kattel, Z. Xie, E. Gomez, P. Liu, J. G. Chen, *Angew. Chem. Int. Ed.* **2015,** *54*, 15501-15505.

[20] F. Solymosi, R. Németh, *Catal. Lett.* **1999,** *62*, 197-200.

[21] T. Baidya, N. Van Vegten, A. Baiker, *Top. Catal.* **2011,** *54*, 881.

[22] J. Zhu, S. Qin, S. Ren, X. Peng, D. Tong, C. Hu, *Catal. Today* **2009,** *148*, 310-315.

[23] J. Lei, R. Justin, O. Naftali, L. Monique, M. D. J., H. Scott, S. S. L., *ChemCatChem* **2009,** *1*, 441-444.

[24] A. Álvarez, M. Borges, J. J. Corral-Pérez, J. G. Olcina, L. Hu, D. Cornu, R. Huang, D. Stoian, A. Urakawa, *ChemPhysChem* **2017,** *18*, 3135-3141.

[25] M. Myint, B. Yan, J. Wan, S. Zhao, J. G. Chen, *J. Catal.* **2016,** *343*, 168-177.

[26] Y. Cheng, L. Zhou, J. Xu, C. Miao, W. Hua, Y. Yue, Z. Gao, *Microporous Mesoporous Mater.* **2016,** *234*, 370-376.

[27] C.-T. Shao, W.-Z. Lang, X. Yan, Y.-J. Guo, *RSC Adv.* **2017,** *7*, 4710-4723.

[28] Z. Xie, B. Yan, J. H. Lee, Q. Wu, X. Li, B. Zhao, D. Su, L. Zhang, J. G. Chen, *Appl. Catal. B* **2019,** *245*, 376-388.

[29] B. Yan, B. Zhao, S. Kattel, Q. Wu, S. Yao, D. Su, J. G. Chen, *J. Catal.* **2019,** *374*, 60-71.

[30] E. Gomez, Z. Xie, J. G. Chen, *AIChE J.* **2019,** *65*, e16670.

[31] S. M. Kim, P. M. Abdala, T. Margossian, D. Hosseini, L. Foppa, A. Armutlulu, W. Van Beek, A. Comas-Vives, C. Coperet, C. Muller, *J Am Chem Soc* **2017,** *139*, 1937-1949.

TOC Graphic

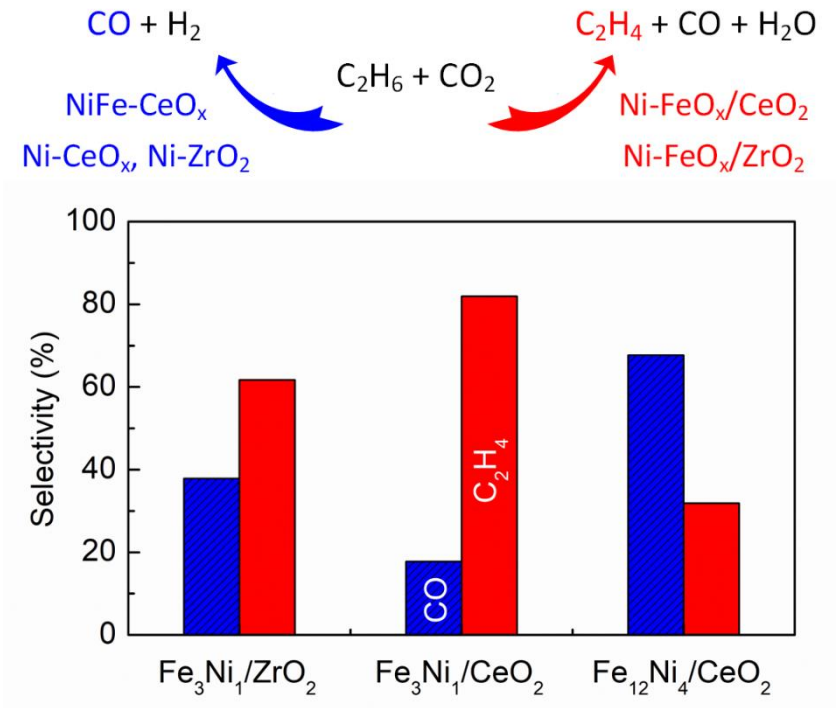

Interfaces determine selectivity: CO_2-assisted oxidative dehydrogenation of ethane can produce CO and ethylene as value-added products over bifunctional supported FeNi catalysts. The high selectivity for CO_2-assisted oxidative dehydrogenation of ethane over Fe_3Ni_1/CeO_2 are likely due to the formation of Ni-FeO_x/CeO_x interfacial sites, while the presence of Ni-ZrO_2 interfacial sites on Fe_3Ni_1/ZrO_2 and NiFe-CeO_x interfacial sites on $Fe_{12}Ni_4/CeO_2$ likely tune the reaction selectivity toward dry reforming of ethane.